Contactless Method to Estimate Antenna Efficiency in a Reverberation Chamber

Contactless Method to Estimate Antenna Efficiency in a Reverberation Chamber

Esmé Galesloot, Anouk Hubrechsen, *IEEE Graduate Student Member*, and Laurens A. Bronckers, *IEEE Member*

***Abstract*—Measuring the efficiency of electrically small antennas and integrated antennas is challenging, since for electrically small antennas, the probe may significantly affect the results and for integrated antennas, establishing a connection with the integrated antenna is in many cases not possible. Therefore, a contactless method to estimate the efficiency of electrically small antennas and integrated antennas is necessary. This paper proposes a novel method to estimate antenna efficiency contactlessly using a reverberation chamber: the contactless efficiency method. In the contactless efficiency method, we combine the two-antenna method with the contactless characterization method, to estimate the *S*-parameters contactlessly. To validate the results, the contactless efficiency method measurements are compared to the measurements of the widely-used two-antenna method and for both methods an uncertainty analysis is performed. Results show a good agreement in the 95% confidence interval between the contactless efficiency method and the existing connectorized method for both the total antenna efficiency and the radiation antenna efficiency. The uncertainty of the contactless efficiency method with a 95% confidence level is below 6% for the whole 0.55 GHz to 1.05 GHz frequency band.**

***Index Terms*—Antenna efficiency, contactless characterization method, contactless efficiency method, reverberation chamber, wireless testing.**

I. Introduction

In recent years, data rate requirements are rapidly increasing, which requires smaller antennas that operate at higher frequencies [1]–[4]. The downside of this, however, is that as the antennas are getting smaller, small manufacturing errors can lead to significant changes in the results of crucial antenna parameters (e.g. gain, mismatch, efficiency) [5]–[7]. Therefore, for electrically small antennas (ESAs) and integrated antennas (IAs), precise characterization is important. A crucial parameter for ESAs and IAs is antenna efficiency, since it has a significant effect on the overall performance of the wireless system. Antennas with a low efficiency may have poor transmission performance or a large power consumption, resulting in a short battery life [8], [9]. Usually, antenna efficiency is measured using a direct connection (e.g. a cable, probe, or waveguide) between the vector network analyzer (VNA) and the antenna under test (AUT) [10]–[17]. However, these connections become increasingly challenging at higher frequencies. For example, the use of a probe can influence the measured results of ESAs [18], [19], and for many IAs, it is not possible to separately connect the antenna, since the AUT is integrated in a full system and the AUT may be difficult to reach. Therefore, a method which can estimate antenna efficiency contactlessly is necessary for the characterization of ESAs and IAs.

Extensive research has been performed on connectorized measurements of antenna efficiency in anechoic chambers (ACs) or reverberation chambers (RCs) [10]–[17], [20]–[23], where the latter has been shown to be more suitable for antenna-efficiency measurements due to its flexibility in device placement in the test volume and its ability to perform rapid and low-cost measurements. There are different methods which use the RC to estimate antenna efficiency. Methods exist which use only one antenna [10]–[12], two antennas [13]–[16], and some use three antennas [17], [24]. Contactless methods have been investigated for their anechoic counterpart, where the *S*-parameters in a system can be estimated contactlessly using the contactless characterization method (CCM). The CCM has previously been used for estimating the antenna impedance contactlessly in an AC [25]–[29]. A recent work shows a method to measure antenna efficiency in a contactless manner in a reverberation chamber [30]. However, a significant drawback of this method is that it requires the reflection coefficient of the AUT to be characterized connected to a VNA, making this method not fully contactless.

In this paper, we introduce, for the first time, a fully contactless method, the contactless efficiency method (CEM), to measure the total and radiation antenna efficiencies in an RC which overcomes those drawbacks. We do so by combining the anechoic CCM with elements of the two-antenna reverberation-chamber method. To show a proof of concept to measure the efficiency of IAs and ESAs contactlessly, we show measurements performed between 0.55 and 1.05 GHz using connectorized antennas to be able to have an accurate reference. The structure of this paper is as follows. Section II explains the CEM, including some of the existing methods which form the basis of this method. Section III describes the setup of the measurements. In Section IV, the uncertainties of the CEM and a connected antenna efficiency method are explained. Section V shows the results of the total and radiation efficiencies estimated using the CEM compared to a connected antenna efficiency method and lastly, in Section VI, a conclusion is given.

II. The Contactless Efficiency Method

This section introduces the new contactless efficiency method which is an extension on the RC-based two-antenna method (TAM) and the CCM [13], [25]–[29], [31]. The TAM is a method which can be used to estimate both the total antenna efficiency and the radiation antenna efficiency of a two-antenna setup in an RC, and the CCM is a method which can be used to estimate the *S*-parameters contactlessly of a two-antenna setup in an AC. The combination between

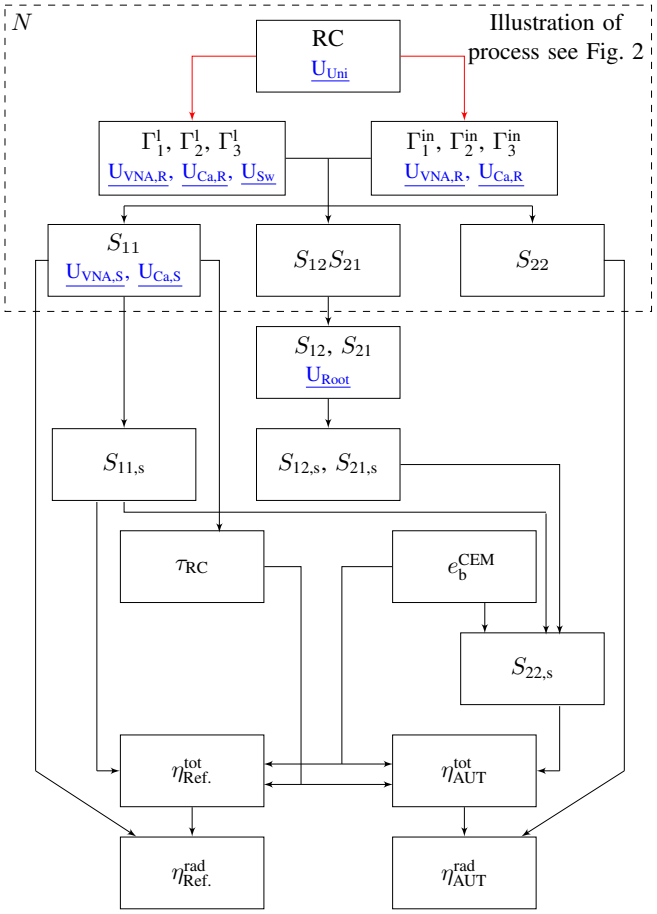

Fig. 1. A block diagram which shows the measurement procedure and the steps on how to estimate the antenna efficiency using the CEM.

the TAM and the CCM is called the CEM. The CEM, as demonstrated in this paper, is a two-antenna method, where only the measurement antenna is connected to the VNA. Note that the efficiency of the measurement antenna does not need to be known. The CEM can be used to contactlessly estimate the total and radiation efficiencies of the AUT in an RC.

Fig. 1 shows the framework that highlights the measurement process of the CEM. It shows step-by-step how we estimate the total and radiation efficiencies of the AUT by performing a contactless measurement using the CEM. These steps are extensively described in the next few subsections. The first steps are depicted by the red arrows, which are the steps where measurements are performed. Then, the *S*-parameters are extracted using the CCM for N mode-stirring samples. This process is highlighted in Fig. 1 with a dashed box and the procedure of the steps inside this dashed box is illustrated in Fig. 2. The rest of the figure shows that these *S*-parameters are applied to a modified version of the two-antenna method. The underlined text shows the uncertainties of the CEM taken into account in this work, which will be further explained in Section IV. For Fig. 1, the section inside the dashed box is based on the CCM and the rest is based on the TAM. However, we extend these methods to estimate efficiency contactlessly using various methods.

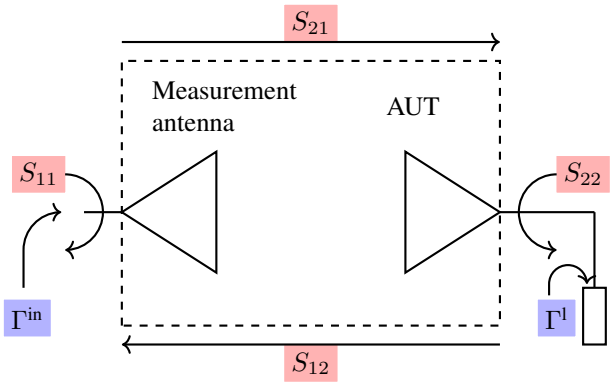

Fig. 2. An illustration of the procedure of the CCM

A. Contactlessly estimate the S-parameters

The first step in the CEM is contactlessly estimating the *S*-parameters for all mode-stirring samples separately using the theory of the CCM. An illustration of this procedure is shown in Fig. 2, by using this setup in the RC, the *S*-parameters can be contactlessly estimated for all mode-stirring samples separately using [28]:

$$\begin{pmatrix} S_{11} \\ S_{22} \\ S_{21}S_{12} - S_{11}S_{22} \end{pmatrix} = \begin{pmatrix} 1 & \Gamma_1^{\text{in}}\Gamma_1^{\text{l}} & \Gamma_1^{\text{l}} \\ 1 & \Gamma_2^{\text{in}}\Gamma_2^{\text{l}} & \Gamma_2^{\text{l}} \\ 1 & \Gamma_3^{\text{in}}\Gamma_3^{\text{l}} & \Gamma_3^{\text{l}} \end{pmatrix}^{-1} \begin{pmatrix} \Gamma_1^{\text{in}} \\ \Gamma_2^{\text{in}} \\ \Gamma_3^{\text{in}} \end{pmatrix}. \quad (1)$$

Here Γ_1^{in}, Γ_2^{in} and Γ_3^{in} are the measured input reflection coefficients, and Γ_1^{l}, Γ_2^{l} and Γ_3^{l} are the measured load reflection coefficients for three different loads. Ideally, these loads are a short, an open and a 50 Ω load, since this will result in the maximum dynamic range. However, any three different loads can be used, as long as the loads are known and sufficiently different. To obtain accurate results, a stable environment between the three Γ^{in} measurements is fundamental. Even though the RC is deterministic per stirrer position [32], a small difference in the stirrer position cannot be excluded. Therefore, for every stirrer position, first Γ_1^{in}, Γ_2^{in} and Γ_3^{in} are measured and then the stirrer moves to the next position. During the CEM measurements, a switch, connected to the AUT is used to switch between a short, an open and a 50 Ω load automatically. Γ^{l} does not depend on the stirrer position and thus only needs to be measured once.

After the measurements of $\Gamma_{1,2,3}^{\text{in}}$ and $\Gamma_{1,2,3}^{\text{l}}$, (1) can be used to estimate S_{11}, S_{22} and $S_{21}S_{12}$ for each stirrer positions separately. Some post processing is required to estimate S_{12} and S_{21} from (1).

B. The complex root of $S_{12}S_{21}$

From (1), $S_{21}S_{12} - S_{11}S_{22}$ can be extracted directly, where S_{12} and S_{21} are assumed to be equal to each other [33]. This assumes the antennas to be reciprocal, however, it is possible to take this constraint into account in active antenna systems by placing a switch between, for example, the antenna and the power amplifier (PA) or low-noise amplifier (LNA). In many systems this switch is already present, where in such a case, the impedance of the PA, the LNA and an open termination

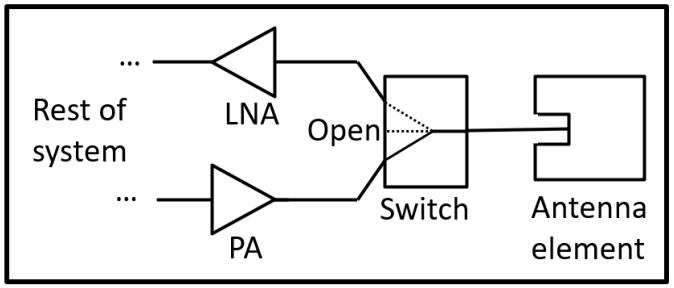

Fig. 3. An illustration of a system with an IA, where the CEM could be used to estimate the antenna efficiency.

could possibly be used as the three different loads. Fig. 3 shows an example of such a possibility, but it should be noted that we only show a proof of concept of an ideal situation with maximum measurable range, and that the concept is yet to be shown in an actual integrated system. These *S*-parameters can be calculated using:

$$S_{12} = S_{21} = \sqrt{S_{21}S_{12}}. \tag{2}$$

The n^{th} root of a complex number can be calculated using [34]:

$$\begin{aligned} &\sqrt[n]{r\mathrm{e}^{\phi i}} = \sqrt[n]{r}\mathrm{e}^{i\theta}, \\ &\text{where } \theta = \frac{\phi}{n} + \frac{2\pi}{n}l, \text{ for } l = 0, 1, \ldots, n-1, \end{aligned} \tag{3}$$

where r is the magnitude and θ the angle of the complex number. Thus, for the second root, which is required to estimate S_{12} and S_{21}, (2) has two unique solutions:

$$\sqrt{r\mathrm{e}^{\phi i}} = \begin{cases} \sqrt{r}\mathrm{e}^{i\frac{\phi}{2}}, & \text{for } l = 0 \\ \sqrt{r}\mathrm{e}^{i(\frac{\phi}{2}+\pi)} = -\sqrt{r}\mathrm{e}^{i\frac{\phi}{2}}, & \text{for } l = 1. \end{cases} \tag{4}$$

For the CEM, it is important to estimate the correct root of S_{12}^2, since this will affect the stirred-energy component of S_{12} ($S_{12,\mathrm{s}}$). Taking only the roots where the real part is positive or the other way around will result in a significant error in $S_{12,\mathrm{s}}$, since the variance on the real axis will be smaller compared to a case where an equal number of samples occur on the positive and negative real axis. Therefore, to estimate the correct root, the distribution of S_{12} has to be taken into account. When the field in the RC is well stirred, the average value of S_{12} is zero[1] [35]:

$$\langle S_{12} \rangle = 0. \tag{5}$$

Furthermore, the real and imaginary parts of S_{12} have a Gaussian distribution [35]. This means that with infinite independent samples exactly 50% of the samples will have a positive real part and 50% will have a negative real part. This also holds for the imaginary part.

With a finite number of samples, as is the case in RC-measurements, the number of samples on the positive or negative side of the real axis will have a binomial distribution with a probability of a sample being on the positive real part of 0.5 [36]. This binomial distribution is given by:

$$\Pr(\text{Samples} = \alpha) = \binom{N}{\alpha} N^{0.5}, \tag{6}$$

where N is the total number of samples and α the number of samples where the real part is positive. This binomial distribution shows that most of the time 50% of the samples will have a positive real part and 50% of the samples will have a negative real part.

To approximate the correct distribution of S_{12}, at each frequency, the samples are randomly split into two groups, each containing 50% of the samples. For the first group, $l = 0$ in (4) to calculate S_{12} in (2) and for the second group, $l = 1$ in (4) to calculate S_{12} in (2), the latter is thus rotated with 180° compared to the solution of $l = 0$. This will result in an S_{12}, where (5) holds. Note that it is still unknown whether the correct root of S_{12} is picked. However, because the samples have low correlation, are randomly spaced around the origin and (5) holds, this will not create a significant error in $\langle |S_{12,\mathrm{s}}|^2 \rangle$, as long as there are a sufficient number of samples. The uncertainty due to this assumption in S_{12} is taken into account in Section IV.

C. Efficiency

This subsection describes how the *S*-parameters are used to calculate efficiency. First, the stirred-energy components of the *S*-parameters ($S_{11,\mathrm{s}}$, $S_{12,\mathrm{s}}$ and $S_{21,\mathrm{s}}$) are estimated, according to [13]. Then, $S_{22,\mathrm{s}}$ is estimated, using the enhanced backscattering coefficient (e_{b}). The parameter e_{b} shows how much of a signal transmitted by a certain antenna is received by the same antenna compared to how much of that signal is received by another antenna in the RC. In an ideal RC, twice as much of the stirred signal is received back by the transmitting antenna compared to the other antenna. Therefore, an ideal RC has an e_{b} equal to two everywhere in the RC [37]. Next, τ_{RC} is estimated, this constant is a measurement of the rate of energy loss in the RC. Finally, the total and radiation efficiencies of both the measurement antenna and the AUT are estimated.

First, $S_{11,\mathrm{s}}$, $S_{12,\mathrm{s}}$ and $S_{21,\mathrm{s}}$ can be estimated using [13]:

$$S_{ij,\mathrm{s}} = S_{ij} - \langle S_{ij} \rangle_N, \tag{7}$$

where i and j are the port indices of the VNA, and N is the number of mode-stirring samples.

Estimating $S_{22,\mathrm{s}}$ using (7) can result in a significant error due to the limited dynamic range [32], and therefore $S_{22,\mathrm{s}}$ is estimated using the assumption that $e_{\mathrm{b}}^{\mathrm{CEM}}$ is equal to two as in the one-antenna method [10]:

$$\langle |S_{22,\mathrm{s}}|^2 \rangle = \frac{(e_{\mathrm{b}}^{\mathrm{CEM}})^2 \langle |S_{12,\mathrm{s}}|^2 \rangle^2}{\langle |S_{11,\mathrm{s}}|^2 \rangle}. \tag{8}$$

To bypass the assumption that $e_{\mathrm{b}}^{\mathrm{CEM}}$ is equal to two, one extra measurement antenna can be used to improve the dynamic range. For example, in such a case, the non-reference three-antenna method [17] or the antenna-replacement method [24], [38] could be used, where the measurement becomes independent of $e_{\mathrm{b}}^{\mathrm{CEM}}$, $S_{11,\mathrm{s}}$, and $S_{22,\mathrm{s}}$. This will be part of future

[1]Note that this may introduce a restriction to the method to only be used in chambers with little to no additional chamber loading, as highly-loaded chambers introduce a high unstirred-energy component.

work. The time constant of the RC (τ_{RC}) is estimated using the linear curve fitting technique, which is described in [39]. To reduce uncertainty, S_{11} is used in the calculation of τ_{RC} since it has the highest signal level. With the S-parameters, its stirred-energy components, the enhanced backscattering coefficient and the time constant, the total efficiency of both antennas can be estimated using [13]:

$$\begin{aligned}\eta_{\text{Ref.}}^{\text{tot}} &= \sqrt{\frac{16\pi^2 V}{\lambda^3}\frac{\langle|S_{11,\text{s}}|^2\rangle}{\omega\tau_{\text{RC}}e_{\text{b}}^{\text{CEM}}}},\\ \eta_{\text{AUT}}^{\text{tot}} &= \sqrt{\frac{16\pi^2 V}{\lambda^3}\frac{e_{\text{b}}^{\text{CEM}}}{\omega\tau_{\text{RC}}}\frac{\langle|S_{12,\text{s}}|^2\rangle^2}{\langle|S_{11,\text{s}}|^2\rangle}},\end{aligned} \tag{9}$$

where V is the volume of the RC (in m^3), λ is the free-space wavelength (in m) and $e_{\text{b}}^{\text{CEM}}$ is assumed to be two. Finally, the radiation efficiency of both the measurement antenna and the AUT can be estimated using [13]:

$$\begin{aligned}\eta_{\text{Ref.}}^{\text{rad}} &= \frac{\eta_{\text{Ref.}}^{\text{tot}}}{1-|\langle S_{11}\rangle|^2},\\ \eta_{\text{AUT}}^{\text{rad}} &= \frac{\eta_{\text{AUT}}^{\text{tot}}}{1-|\langle S_{22}\rangle|^2}.\end{aligned} \tag{10}$$

Next, we introduce the measurement setup of the CEM and the TAM in the RC, which is used to compare the results of the CEM to the TAM.

III. Measurement Setup

In this section the measurement setups to validate the results of the CEM compared to the TAM are described. To accurately verify the results of the CEM, the AUT used in the CEM is a connectorized antenna, such that its efficiency can also be estimated using the TAM. Therefore, this section describes the setup of two types of measurements. Where both setups are almost identical, however, for the TAM, the AUT is connected to the VNA, and for the CEM, the AUT is connected to a switch. A drawing of the setup of the CEM is shown in Fig. 4. Pictures of the setup of the TAM at the Eindhoven University of Technology (TU/e) are shown in Fig. 5 and pictures of the setup of the CEM at the TU/e are shown in Fig. 6, where Fig. 6a shows the measurement antenna and Fig. 6a shows the AUT. The switch connected to the AUT is clearly visible.

Both the TAM and the CEM are performed with the same settings and equipment. The measurements are performed in the RC at the TU/e, which dimensions are: 4.05 m by 5.7 m by 3.15 m. This RC stirs the field with the use of an oscillating-wall stirrer, which is described in [40]. Measurements are performed between 0.55 GHz and 1.05 GHz, with 10001 frequency steps. Furthermore, during the measurements an IF bandwidth of 1 kHz is used and the VNA output power is set to 12 dBm.

During these measurements, two log-periodic antennas are used, a silver ETS-Lindgren EMCO 3146 antenna and a blue Teseq UPA 6109 antenna. Both antennas are suitable within the band of interest. The silver antenna is shown in Fig 6a and the blue antenna is shown in Fig 6b. The VNA used during the measurements is the Rohde and Schwarz ZNB20 Vector

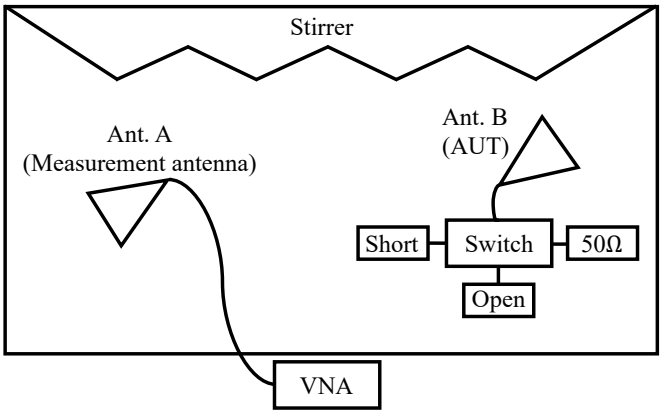

Fig. 4. The setup of the CEM in the RC to estimate antenna efficiency.

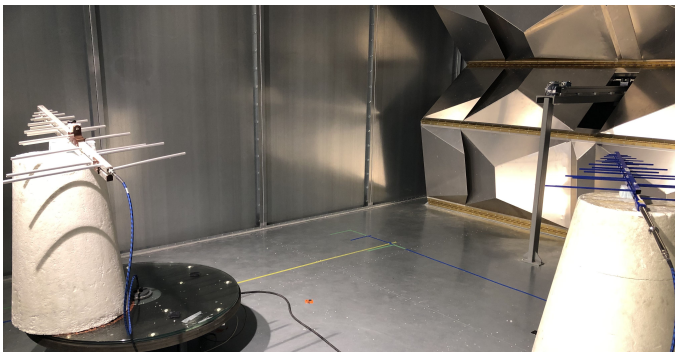

Fig. 5. The setup of the TAM in the RC at the TU/e.

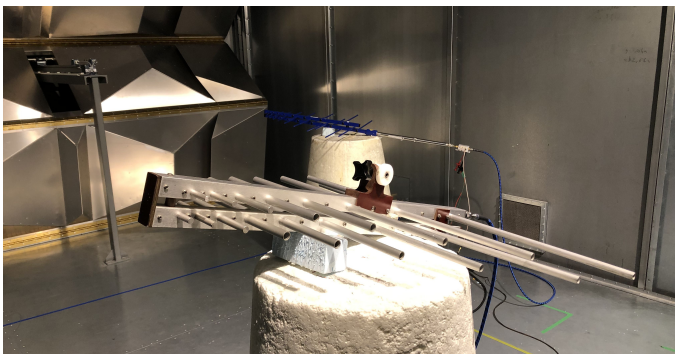

(a) The measurement antenna

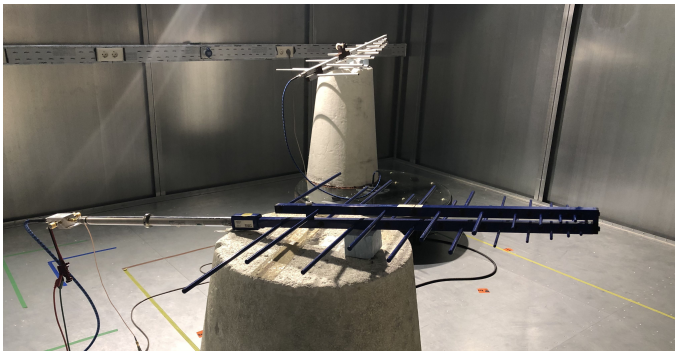

(b) The AUT including the switch

Fig. 6. The setup of the CEM in the RC at the TU/e.

TABLE I. The stirring sequence of the independent realizations to estimate the uncertainty due to lack of spatial uniformity

		Turntable				Paddle
IR	**Height**	**Angles**			Number of positions	Number of positions
1	0 m	0°,	120°,	240°	3	33
2	0 m	30°,	150°,	270°	3	33
3	0 m	60°,	180°,	300°	3	33
4	0 m	90°,	210°,	330°	3	33
5	0.6 m	0°,	120°,	240°	3	33
6	0.6 m	30°,	150°,	270°	3	33
7	0.6 m	60°,	180°,	300°	3	33
8	0.6 m	90°,	210°,	330°	3	33

Network Analyzer. For the calibration, a 3.5 mm TC-CK-35 calibration kit from TactiCal is used. The cables used during the measurements are cables with 3.5 mm precision connectors and extra phase stability, suitable up to 26.5 GHz. The switch, which is only used during the CEM, is the Mini-Circuits ZSDR-425+ switch. This is a four way switch, suitable for frequencies between 10 MHz and 2.5 GHz. The three different loads connected to the switch during the CEM are the short, open and 50 Ω load from the TactiCal 3.5 mm TC-CK-35 calibration kit. By applying 0 V or 5 V to the ports, the switch can be changed to one of the four ports.

The stirring mechanism consists of a paddle, which stirs the field by changing its position and a turntable, which stirs the field by position stirring. The measurement antenna is on top of the turntable. The measurements are performed with 33 paddle positions, 12 turntable angles and 2 antenna heights, resulting in 892 mode-stirring samples. For this stirring sequence, the correlation between each stepped paddle position and turntable angle is lower than the threshold of 0.5, verifying sample independence [41]–[44].

The measurements with 892 mode-stirring samples can be split into independent realizations. Each independent realization requires a minimum number of mode-stirring samples to obtain reliable results. Splitting the measurements into eight independent realizations, will give each independent realization 99 mode-stirring samples, which is a sufficient number of mode-stirring samples for each independent realization to obtain reliable results [32], [43], [45]. Table I shows that each independent realization uses all 33 paddle positions, three out of the twelve turntable angles and either the original height of the measurement antenna or a position 0.6 m higher, resulting in 99 mode-stirring samples for each independent realization. Lastly, to prove the concept of the CEM, these measurements are performed for two different setups. Setup 1, where the blue antenna is the AUT and the silver antenna is the measurement antenna, and Setup 2, where the silver antenna is the AUT and the blue antenna is the measurement antenna. In the end, for both the TAM and the CEM, four different measurements are performed.

1) Measurement $\eta_{\text{Tot,S1}}$: estimating the total efficiency of the AUT in Setup 1,
2) Measurement $\eta_{\text{Tot,S2}}$: estimating the total efficiency of the AUT in Setup 2,
3) Measurement $\eta_{\text{Rad,S1}}$: estimating the radiation efficiency of the AUT in Setup 1,
4) and Measurement $\eta_{\text{Rad,S2}}$: estimating the radiation efficiency of the AUT in Setup 2.

TABLE II. Uncertainties of the TAM and the CEM

	Uncertainty	**TAM**	**CEM**
	$\underline{\text{U}_{\text{Uni}}}$: Uniformity	✓	✓
$\underline{\text{U}_{\text{MC}}}$	$\underline{\text{U}_{\text{VNA,R}}}$: VNA (random)	✓	✓
	$\underline{\text{U}_{\text{VNA,S}}}$: VNA (systematic)	✓	✓
	$\underline{\text{U}_{\text{Ca,R}}}$: Cable (random)	✓	✓
	$\underline{\text{U}_{\text{Ca,S}}}$: Cable (systematic)	✓	✓
	$\underline{\text{U}_{\text{Sw}}}$: Switch		✓
	$\underline{\text{U}_{\text{Root}}}$: Complex root of S_{12}		✓

IV. Uncertainty Analysis

In this section, the uncertainties taken into account for both the TAM and the CEM are described. Table II and Fig. 1 shows the uncertainties of both the TAM and the CEM.

Uncertainty $\underline{\text{U}_{\text{Uni}}}$ is the uncertainty due to lack of spatial uniformity in the RC [35], [46]. The standard uncertainty due to lack of spatial uniformity is estimated via the standard deviation between different independent realizations. This is therefore a Type A uncertainty. Uncertainty $\underline{\text{U}_{\text{VNA}}}$ is the uncertainty due to the VNA. This uncertainty exist of a component of uncertainty arising from a random effect ($\underline{\text{U}_{\text{VNA,R}}}$) and a component of uncertainty arising from a systematic effect ($\underline{\text{U}_{\text{VNA,S}}}$), the latter is constant with respect to time. $\underline{\text{U}_{\text{VNA,S}}}$ and $\underline{\text{U}_{\text{VNA,R}}}$ are both obtained via the datasheet of the VNA [47] and are therefore a Type B uncertainty. $\underline{\text{U}_{\text{VNA,R}}}$ is also validated via a series of measurements. For the CEM, $\underline{\text{U}_{\text{VNA,S}}}$ will only affect S_{11}, since the systematic offset will cancel out in the calculation of S_{12}, S_{21}, and S_{22}.

Uncertainty $\underline{\text{U}_{\text{Ca}}}$ is the uncertainty due to the cables. This uncertainty consists of a component of uncertainty arising from a random effect ($\underline{\text{U}_{\text{Ca,R}}}$) and a component of uncertainty arising from a systematic effect ($\underline{\text{U}_{\text{Ca,S}}}$). Both components are estimated via the manufacturer website [48] and are therefore a Type B uncertainty. Also for the cables, $\underline{\text{U}_{\text{Ca,S}}}$ will only affect S_{11} for the CEM.

Uncertainty $\underline{\text{U}_{\text{Sw}}}$ is the uncertainty due to the switch, which is connected to the AUT. This uncertainty is measured via a series of measurements and is therefore a Type A uncertainty.

Lastly, there is also an uncertainty due to the complex-root assumption of S_{12}. As explained in Section II-B, S_{12} has a binomial distribution in the number of samples which have a positive real component. During post-processing of the measurements it is assumed that 50% of the samples have a positive real component and 50% a negative real component. However, since there is a finite number of samples this is not always the case. Uncertainty $\underline{\text{U}_{\text{Root}}}$ is the uncertainty due to the assumption that exactly 50% of the samples have a positive real component and 50% a negative real component, this is a Type A uncertainty.

TABLE III. The average standard deviation of the different components contributed to the combined standard uncertainty on the total and radiation efficiencies and the combined uncertainty with a 95% confidence level.

		TAM		CEM	
$\underline{U_{Uni}}$	Tot. Eff.	1.70 %	0.08 dB	1.70 %	0.09 dB
	Rad. Eff.	1.73 %	0.08 dB	1.73 %	0.09 dB
$\underline{U_{MC}}$	Tot. Eff.	0.03 %	$<$ 0.01 dB	0.14 %	$<$ 0.01 dB
	Rad. Eff.	0.03 %	$<$ 0.01 dB	0.14 %	$<$ 0.01 dB
$\underline{U_C}$	Tot. Eff.	3.93 %	0.19 dB	3.98 %	0.20 dB
	Rad. Eff.	4.00 %	0.19 dB	4.04 %	0.20 dB

Fig. 1 shows that for the CEM, $\underline{U_{VNA,R}}$, $\underline{U_{Ca,R}}$ and $\underline{U_{Sw}}$ affect Γ_S^l, Γ_O^l and Γ_L^l, $\underline{U_{VNA,R}}$, $\underline{U_{Ca,R}}$ affect Γ_S^{in}, Γ_O^{in}, Γ_L^{in}, and $\underline{U_{VNA,S}}$, $\underline{U_{Ca,S}}$ affect S_{11} for the CEM. To estimate the uncertainty, a Gaussian random variable of the previous stated uncertainties is added in the Monte Carlo method [49]. $\underline{U_{Root}}$ affects S_{12} and S_{21}. In contrast to the uncertainties given before, $\underline{U_{Root}}$ has a binomial distribution in stead of a Gaussian distribution. To include this uncertainty, a random binomial variable with a distribution of (6) is picked, where $N = 396$ for this measurement setup. This random variable shows how many randomly picked samples of S_{12} are positive in the real part. The rest of the samples of S_{12} are rotated with 180° and thus negative in the real part. Using the Monte Carlo method, which is run 100 times, a standard uncertainty of the efficiency ($\underline{U_{MC}}$) can be obtained, which includes the VNA, cables, switch and complex-root assumption of S_{12}.

As explained, the uncertainty due to lack of spatial uniformity is estimated by measuring antenna efficiency for eight independent realizations and the uncertainty on antenna efficiency due to the VNA, cables, switch and the complex-root assumption of S_{12} is estimated using the Monte Carlo method. We isolated $\underline{U_{Uni}}$ to show that the expanded uncertainty is dominated by this component. The combined uncertainty can be obtained using the root-sum-of-squares technique [50], [51]:

$$\underline{U_c} = k\sqrt{\underline{U_{Uni}^2} + \underline{U_{MC}^2}}, \tag{11}$$

where k is the coverage factor. The coverage factor depends on the desired confidence level and the effective degrees of freedom. Note that $\underline{U_{MC}}$ consists of multiple Type A and Type B uncertainties, as shown in Table II. In this paper k is chosen such that (11) gives the uncertainty with a 95% confidence level and the effective degrees of freedom can be calculated using the Welch-Satterthwaite equation [50], [51]. Depending on the frequency the effective degrees of freedom where 8 and 9 corresponding to the coverage factors 2.31 and 2.26, respectively. In the following section the results of the TAM and the CEM, including the uncertainty of these methods, are compared.

V. Results

The estimated total and radiation efficiencies for both the TAM and CEM for two setups are shown in Fig. 7. The red results are from the TAM and the blue results from the CEM. The semi-transparent surfaces show the combined uncertainties of both the TAM and the CEM with a confidence level of 95%. Fig. 7a shows, the estimated total efficiency of the AUT in Setup 1, $\eta_{Tot,S1}$, Fig. 7b shows the estimated total efficiency of the AUT in Setup 2, $\eta_{Tot,S2}$, Fig. 7c shows the estimated radiation efficiency of the AUT in Setup 1, $\eta_{Rad,S1}$ and lastly, Fig. 7d shows the estimated radiation efficiency of the AUT in Setup 2, $\eta_{Rad,S2}$. As Fig. 7a shows, for $\eta_{Tot,S1}$ the difference between the result of the TAM and the CEM is over this frequency range on average 1.0%. While the deviation between the best estimates of Setup 2 is larger than in Setup 1, the 95% confidence bounds of the TAM and CEM overlap for all frequency samples, showing that there is no statistically distinguishable between the two. The latter also holds for the results of $\eta_{Tot,S2}$, $\eta_{Rad,S1}$ and $\eta_{Rad,S2}$.

Table III shows the contribution of the different components to the combined standard uncertainty and the combined uncertainty with a 95% confidence level. For the TAM, $\underline{U_{Uni}}$ is the uncertainty due to lack of spatial uniformity and $\underline{U_{MC}}$ consists of the uncertainty due to the VNA and the cables. Note that $\underline{U_{Uni}}$ and $\underline{U_{MC}}$ in this table shows the standard uncertainty. Furthermore, $\underline{U_{MC}}$ is less then 0.01 dB. Even though this uncertainty is very small, it is taken into account in the uncertainty analysis. As Table III shows, the uncertainty estimated via the Monte Carlo method is four to fives times higher for the CEM than the TAM. The uncertainty estimated via the Monte Carlo method of the CEM is higher compared to the TAM, because for CEM the signal measured by the VNA includes all *S*-parameters, where for the TAM this signal includes only one *S*-parameter. Therefore, $\underline{U_{VNA}}$ and $\underline{U_{Ca}}$ have a higher effect on the results of the CEM compared to the TAM. Furthermore, the uncertainty of the CEM includes $\underline{U_{Sw}}$ and $\underline{U_{Root}}$, which is not the case for the TAM. However, the uncertainty due to lack of spatial uniformity in the RC is still significantly higher than the uncertainty estimated via the the Monte Carlo method for both the TAM and the CEM. As Table III shows, the combined uncertainty of the CEM compared to the TAM is on average below 0.05%. As an additional part of the proof-of-concept, the results of the best estimate of $|\langle S_{22}\rangle|$ and $\langle|S_{22,s}|^2\rangle$ estimated using the TAM and CEM for both setups are shown in Fig. 8, where Fig. 8a shows the results of Setup 1 and Fig. 8b shows the results of Setup 2. Fig. 8a and Fig. 8b show that the estimated $\langle|S_{22,s}|^2\rangle$ has a relative mean error of 0.22 dB and 0.40 dB for Setup 1 and 2, respectively. Considering that both setups have an uncertainty of approximately 0.2 dB, they are within each others uncertainty bounds, showing a good agreement between the best estimates of the TAM and the CEM. For the measured reflection coefficient, this error is larger, approximately 0.49 dB and 1.00 dB for Setup 1 and 2, respectively. However, note that this does not lead to an equally large deviation in radiation efficiency, as is shown in Fig. 7, demonstrating the effectivity of this method.

The results shown in Fig. 7, Table III and Fig. 8 verify that the CEM can be an accurate method to estimate antenna efficiency contactlessly at low frequencies. Furthermore, for the TAM, e_b is between 1.95 and 2.16 over the whole fre-

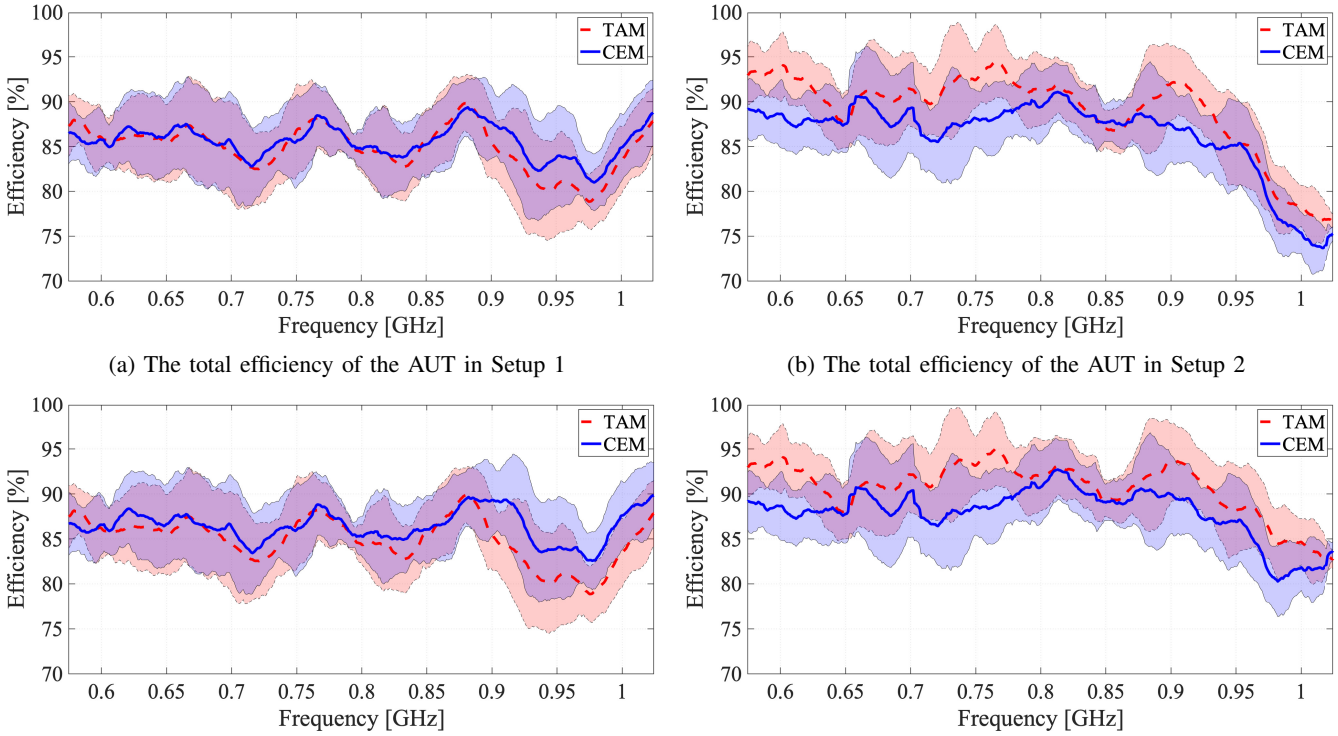

(a) The total efficiency of the AUT in Setup 1

(b) The total efficiency of the AUT in Setup 2

(c) The radiation efficiency of the AUT in Setup 1

(d) The radiation efficiency of the AUT in Setup 2

Fig. 7. Results of the estimated total and radiation efficiencies of the AUT via the CEM compared to the TAM for two different setups with a confidence level of 95%. The 95% confidence intervals overlap for all setups for the total and radiation efficiencies over the full frequency band, demonstrating that the CEM can be used to accurately estimate the efficiency of ESAs and IAs.

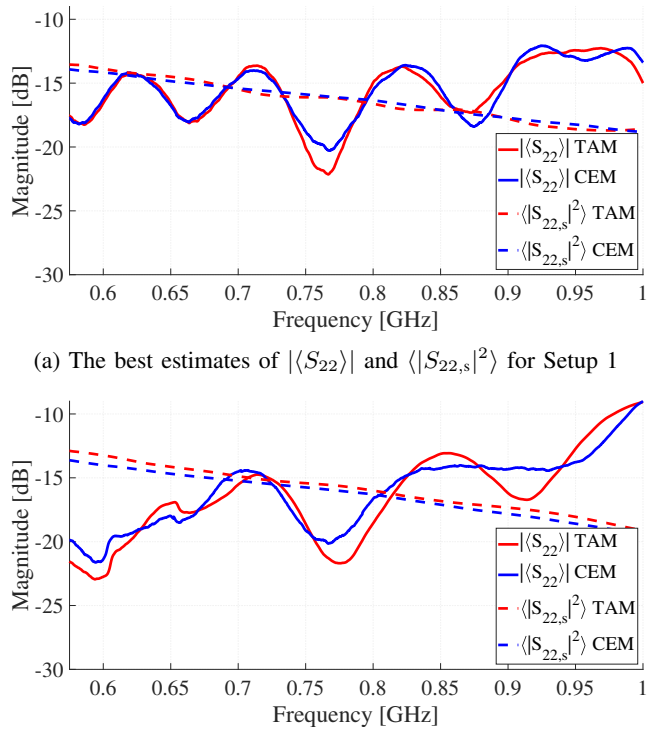

(a) The best estimates of $|\langle S_{22}\rangle|$ and $\langle|S_{22,s}|^2\rangle$ for Setup 1

(b) The best estimates of $|\langle S_{22}\rangle|$ and $\langle|S_{22,s}|^2\rangle$ for Setup 2

Fig. 8. The best estimates of $|\langle S_{22}\rangle|$ and $\langle|S_{22,s}|^2\rangle$ estimated using the CEM and the TAM for two different setups.

quency band, with an average of 2.06, making the assumption that $e_{\mathrm{b}}^{\mathrm{CEM}}$ is equal to two an acceptable assumption. It should be noted that, since the full S-parameter matrix is estimated using this method, it should also be applicable to other antenna-efficiency methods. Additionally, as mentioned earlier, a three-antenna method could be applied with an additional measurement antenna, making the method independent of $e_{\mathrm{b}}^{\mathrm{CEM}}$. More research is required to estimate the uncertainty of the CEM for low-efficiency antennas or when using less-ideal loads, because in those situations the dynamic range is lower compared to the measurement setup described in this paper. The dynamic range can be a limitation using the CEM. Therefore, considering a high output power of the VNA, it is expected that this method can be applicable for characterization of IAs and EAs at mm-wave frequencies.

VI. Conclusion

In this paper we introduced a novel method, the CEM, that can be used to contactlessly estimate the total and radiation antenna efficiencies in a reverberation chamber. Measurements showed an agreement within the uncertainty bounds between the CEM and an existing connectorized measurement method, where for the CEM the combined uncertainty was below 6.0% and for the connectorized measurement method below 5.7% over the whole 0.55 GHz to 1.05 GHz frequency band. With these results, estimating the efficiency of electrically-small and integrated antennas accurately can be achievable using the CEM. In future work, we will use two measurement antennas

in the CEM to bypass the assumption of $e_{\mathrm{b}}^{\mathrm{CEM}}$ being equal to two and to improve the dynamic range. Furthermore, in future publications, we will apply the CEM to (integrated) antennas operating at higher frequencies and to antennas with lower efficiencies.

REFERENCES

[1] F. Jejdling, "Ericsson mobility report," *Ericsson*, November 2021.

[2] D. Soldani and A. Manzalini, "Horizon 2020 and beyond: On the 5g operating system for a true digital society," *IEEE Vehicular Technology Magazine*, vol. 10, no. 1, pp. 32–42, 2015.

[3] T. Huang, W. Yang, J. Wu, J. Ma, X. Zhang, and D. Zhang, "A survey on green 6g network: Architecture and technologies," *IEEE Access*, vol. 7, pp. 175 758–175 768, 2019.

[4] K. David and H. Berndt, "6g vision and requirements: Is there any need for beyond 5g?" *IEEE Vehicular Technology Magazine*, vol. 13, no. 3, pp. 72–80, 2018.

[5] J. Spurek and Z. Raida, "Sensitivity analysis of a modular circularly polarized antenna array for 60 ghz band," in *2020 23rd International Microwave and Radar Conference (MIKON)*, 2020, pp. 56–60.

[6] M. Abbas-Azimi, F. Arazm, and J. Rashed-Mohassel, "Sensitivity analysis of a 1 to 18 ghz broadband drgh antenna," in *2006 IEEE Antennas and Propagation Society International Symposium*, 2006, pp. 3129–3132.

[7] J. Martens, "Mm-wave partial information de-embedding: Errors and sensitivities," in *2018 91st ARFTG Microwave Measurement Conference (ARFTG)*, 2018, pp. 1–4.

[8] A. Azremi, H. Ghafouri Shiraz, and P. S. Hall, "Reverberation chamber for efficiency measurement of small antennas," in *2005 1st International Conference on Computers, Communications, Signal Processing with Special Track on Biomedical Engineering*, 2005, pp. 25–29.

[9] T. H. Loh and J. Li, "The effect of receiving antenna orientation and polarization on measurements of antenna efficiency in a reverberation chamber," in *2017 11th European Conference on Antennas and Propagation (EUCAP)*, 2017, pp. 3743–3746.

[10] C. L. Holloway, R. Smith, C. Dunlap, R. Pirkl, J. Ladbury, W. Young, B. Hansell, M. Shadish, and K. Sullivan, "Validation of a one-antenna reverberation-chamber technique for estimating the total and radiation efficiency of an antenna," in *2012 IEEE International Symposium on Electromagnetic Compatibility*, 2012, pp. 205–209.

[11] N. Pires, C. Mendes, M. Koohestani, A. K. Skrivervik, and A. A. Moreira, "Novel approach to the measurement of ultrawideband antenna efficiency," *IEEE Antennas and Wireless Propagation Letters*, vol. 12, pp. 1512–1515, 2013.

[12] C. S. Lee, A. Duffy, and C. Lee, "Antenna efficiency measurements in a reverberation chamber without the need for a reference antenna," *IEEE Antennas and Wireless Propagation Letters*, vol. 7, pp. 448–450, 2008.

[13] C. L. Holloway, R. S. Smith, C. R. Dunlap, R. J. Pirkl, J. Ladbury, W. F. Young, D. A. Hill, W. R. Hansell, M. A. Shadish, and K. B. Sullivan, "Validation of a two-antenna reverberation-chamber technique for estimating the total and radiation efficiency of antennas," in *International Symposium on Electromagnetic Compatibility - EMC EUROPE*, 2012, pp. 1–6.

[14] Q. Xu, Y. Huang, X. Zhu, L. Xing, Z. Tian, and C. Song, "A modified two-antenna method to measure the radiation efficiency of antennas in a reverberation chamber," *IEEE Antennas and Wireless Propagation Letters*, vol. 15, pp. 336–339, 2016.

[15] C. Li, T.-H. Loh, Z. H. Tian, Q. Xu, and Y. Huang, "A comparison of antenna efficiency measurements performed in two reverberation chambers using non-reference antenna methods," in *2015 Loughborough Antennas Propagation Conference (LAPC)*, 2015, pp. 1–5.

[16] A. Khaleghi, "Time-domain measurement of antenna efficiency in reverberation chamber," *IEEE Transactions on Antennas and Propagation*, vol. 57, no. 3, pp. 817–821, 2009.

[17] C. L. Holloway, H. A. Shah, R. Pirkl, W. F. Young, D. A. Hill, and J. Ladbury, "A three-antenna technique for determining the total and radiation efficiencies of antennas in reverberation chambers," *IEEE Antennas and Propagation Magazine*, vol. 54, no. 1, pp. 235–241, 2012.

[18] A. C. F. Reniers, A. R. van Dommele, M. D. Huang, and M. H. A. J. Herben, "Disturbing effects of microwave probe on mm-wave antenna pattern measurements," in *The 8th European Conference on Antennas and Propagation (EuCAP 2014)*, 2014, pp. 161–164.

[19] Z. Zheng, Y. Zhang, L. Shi, L. Wu, and J.-F. Mao, "An overview of probe-based millimeter-wave/terahertz far-field antenna measurement setups [measurements corner]," *IEEE Antennas and Propagation Magazine*, vol. 63, no. 2, pp. 63–118, 2021.

[20] C. L. Holloway, H. A. Shah, R. J. Pirkl, W. F. Young, D. A. Hill, and J. Ladbury, "Reverberation chamber techniques for determining the radiation and total efficiency of antennas," *IEEE Transactions on Antennas and Propagation*, vol. 60, no. 4, pp. 1758–1770, 2012.

[21] W. Krouka, F. Sarrazin, J. Sol, P. Besnier, and E. Richalot, "Comparison of antenna radiation efficiency measurement techniques in reverberation chamber using or not a reference antenna," in *2020 14th European Conference on Antennas and Propagation (EuCAP)*, 2020, pp. 1–4.

[22] N. Serafimov, P.-S. Kildal, and T. Bolin, "Comparison between radiation efficiencies of phone antennas and radiated power of mobile phones measured in anechoic chambers and reverberation chamber," in *IEEE Antennas and Propagation Society International Symposium*, vol. 2, 2002, pp. 478–481.

[23] T.-H. Loh and W. Qi, "A comparison of mimo antenna efficiency measurements performed in anechoic chamber and reverberation chamber," in *2015 85th Microwave Measurement Conference (ARFTG)*, 2015, pp. 1–4.

[24] A. Hubrechsen, K. A. Remley, and S. Catteau, "Reverberation chamber metrology for wireless internet of things devices: Flexibility in form factor, rigor in test," *IEEE Microwave Magazine*, vol. 23, no. 2, pp. 75–85, 2022.

[25] A. van den Biggelaar, D. Daverveld, A. Reniers, U. Johannsen, and A. Smolders, "Assessment of a contactless characterization method for integrated antennas," in *2019 49th European Microwave Conference (EuMC)*, 2019, pp. 1016–1019.

[26] A. J. Van Den Biggelaar, E. Galesloot, A. C. Franciscus, A. B. Smolders, and U. Johannsen, "Verification of a contactless characterization method for millimeter-wave integrated antennas," *IEEE Transactions on Antennas and Propagation*, vol. 68, no. 5, pp. 3358–3365, 2020.

[27] U. Johannsen, M. Spiritoy, and A. Smolders, "Contactless measurement method for integrated mm-wave antennas," in *Proceedings of the 5th European Conference on Antennas and Propagation (EUCAP)*, 2011, pp. 797–801.

[28] B. Monsalve, S. Blanch, J. Romeu, and L. Jofre, "A contact-less small antenna characterization through impedance modulation," in *2009 3rd European Conference on Antennas and Propagation*, 2009, pp. 696–698.

[29] S. Bories, M. Hachemi, K. H. Khlifa, and C. Delaveaud, "Small antennas impedance and gain characterization using backscattering measurements," in *Proceedings of the Fourth European Conference on Antennas and Propagation*, 2010, pp. 1–5.

[30] W. Krouka, F. Sarrazin, J. d. Rosny, A. Labdouni, and E. Richalot, "Antenna radiation efficiency estimation from backscattering measurement performed within reverberation chambers," *IEEE Transactions on Electromagnetic Compatibility*, vol. 64, no. 2, pp. 267–274, 2022.

[31] "Ieee recommended practice for antenna measurements," *IEEE Std 149-2021 (Revision of IEEE Std 149-1977)*, pp. 115–116, 2022.

[32] A. Hubrechsen, K. A. Remley, R. D. Jones, D. F. Williams, D. Gu, A. B. Smolders, and L. A. Bronckers, "The effect of noise on reverberation-chamber measurements of antenna efficiency," *IEEE Transactions on Antennas and Propagation*, vol. 69, no. 12, pp. 8744–8752, 2021.

[33] M. Neiman, "The principle of reciprocity in antenna theory," *Proceedings of the IRE*, vol. 31, no. 12, pp. 666–671, 1943.

[34] T. Andreescu, D. Andrica *et al.*, *Complex Numbers from A to... Z*. Springer, 2006, vol. 165.

[35] D. A. Hill, *Electromagnetic fields in cavities: deterministic and statistical theories*. John Wiley & Sons, 2009, vol. 35.

[36] E. Von Collani and K. Dräger, *Binomial distribution handbook for scientists and engineers*. Springer Science & Business Media, 2001.

[37] J. Ladbury and D. A. Hill, "Enhanced backscatter in a reverberation chamber: Inside every complex problem is a simple solution struggling to get out," in *2007 IEEE International Symposium on Electromagnetic Compatibility*, 2007, pp. 1–5.

[38] "Electromagnetic compatibility (EMC) part 4: Testing and measurement techniques; section 21: Reverberation chamber test methods," International Electrotechnical Comission, Geneva, Switzerland, Tech. Rep. IEC 61000-4-21, 2001.

[39] X. Zhang, M. Robinson, and I. Flintoft, "On measurement of reverberation chamber time constant and related curve fitting techniques," in *2015 IEEE International Symposium on Electromagnetic Compatibility (EMC)*, 2015, pp. 406–411.

[40] D. Barakos and R. Serra, "Performance characterization of the oscillating wall stirrer," in *2017 International Symposium on Electromagnetic Compatibility - EMC EUROPE*, 2017, pp. 1–4.

[41] A. Hubrechsen, K. A. Remley, R. D. Jones, R. D. Horansky, V. T. Neylon, and L. A. Bronckers, "Nb-iot devices in reverberation chambers: a comprehensive uncertainty analysis," *International Journal of Microwave and Wireless Technologies*, vol. 13, no. 6, pp. 561–568, 2021.
[42] K. A. Remley, C.-M. J. Wang, D. F. Williams, J. J. aan den Toorn, and C. L. Holloway, "A significance test for reverberation-chamber measurement uncertainty in total radiated power of wireless devices," *IEEE Transactions on Electromagnetic Compatibility*, vol. 58, no. 1, pp. 207–219, 2016.
[43] R. J. Pirkl, K. A. Remley, and C. S. L. Patané, "Reverberation chamber measurement correlation," *IEEE Transactions on Electromagnetic Compatibility*, vol. 54, no. 3, pp. 533–545, 2012.
[44] M. G. Becker, M. Frey, S. Streett, K. A. Remley, R. D. Horansky, and D. Senic, "Correlation-based uncertainty in loaded reverberation chambers," *IEEE Transactions on Antennas and Propagation*, vol. 66, no. 10, pp. 5453–5463, 2018.
[45] L. A. Bronckers, K. A. Remley, B. F. Jamroz, A. Roc'h, and A. Bart Smolders, "Uncertainty in reverberation-chamber antenna-efficiency measurements in the presence of a phantom," *IEEE Transactions on Antennas and Propagation*, vol. 68, no. 6, pp. 4904–4915, 2020.
[46] D. Senic, K. A. Remley, M. G. Becker, and C. L. Holloway, "Spatial uniformity study in a loaded reverberation chamber at millimeter-wave frequencies," in *2018 IEEE Symposium on Electromagnetic Compatibility, Signal Integrity and Power Integrity (EMC, SI PI)*, 2018, pp. 467–472.
[47] Rohde&Schwarz, *RS®ZNB Vector Network Analyzer Specifications*, April 2021, version 03.00.
[48] Junkosha. 0 series - precision test grade phase stability. [Online]. Available: https://www.junkosha.com/en/products/EMF-00
[49] R. Y. Rubinstein and D. P. Kroese, *Simulation and the Monte Carlo method*. John Wiley & Sons, 2016, vol. 10.
[50] B. N. Taylor, C. E. Kuyatt *et al.*, "Guidelines for evaluating and expressing the uncertainty of nist measurement results," 1994.
[51] J. Jcgm *et al.*, "Evaluation of measurement data—guide to the expression of uncertainty in measurement," *Int. Organ. Stand. Geneva ISBN*, vol. 50, p. 134, 2008.

Esmé Galesloot received the B.Sc. and M.Sc. degrees (cum laude) in Electrical Engineering from the Eindhoven University of Technology (TU/e), Eindhoven, The Netherlands, in 2019 and 2021, respectively, where she specialized in antenna design and metrology. In 2020, she was a guest researcher at Chalmers University of Technology, working on gapwave technology for antenna design. She is currently working with Philips Engineering Solutions in the RF and EMC group as an RF designer.

Anouk Hubrechsen (Graduate Student Member, IEEE) received the B.Sc. and M.Sc. degrees in electrical engineering from the Eindhoven University of Technology, Eindhoven, The Netherlands, in 2017 and 2019, respectively, where she is currently pursuing a Ph.D. degree. She was a Guest Researcher with the National Institute of Standards and Technology at Boulder, Boulder, CO, USA, in 2018 and 2019, where she was involved in reverberation-chamber metrology for Internet-of-Things applications. She is currently involved in a project on reverberation-chamber metrology for 5G-and-beyond mm-wave applications and she is CEO of AntenneX B.V.. Hubrechsen received the Regional and District Zonta Women in Technology Awards, in 2019. From 2020 to 2021, she was the Vice-Chair of IEEE Benelux Women in Engineering.

Laurens A. (Sander) Bronckers received the M.Sc. degree (cum laude) in electrical engineering from Eindhoven University of Technology (TU/e), The Netherlands, in 2015. In 2018, he was a visiting researcher at NIST (Boulder, Colorado) on antenna measurements in reverberation chambers. He obtained the Ph.D. degree (cum laude) in electrical engineering in 2019, within the electromagnetics group at TU/e, on design and measurement techniques for next-generation integrated antennas. Since 2019, he is an assistant professor on Metrology for Antennas and Wireless Systems at TU/e. In addition, he chairs the ultra high data rate track in the Centre for Wireless Technology Eindhoven (CWT/e). In 2020, he co-founded AntenneX BV, a spin-off focusing on high-frequency wireless characterization. His research interests include antenna (system) measurements in reverberation and hybrid chambers, channel sounding and emulation, and RF material characterization.